

Assimilation of current measurements into a circulation model of Lake Michigan

Zepu Zhang,¹ Dmitry Beletsky,² David J. Schwab,³ and Michael L. Stein⁴

Received 9 December 2006; revised 12 July 2007; accepted 1 August 2007; published 7 November 2007.

[1] We present a method for assimilating current observations into a two-dimensional circulation model of Lake Michigan, based on the Princeton Ocean Model (POM) and driven by observed winds. Because measurements of surface level are not available, we require that the point-wise update to the forecast horizontal current does not change the forecast surface level. This requirement makes it possible to represent the current updates by a stream function. Given an appropriate covariance model of this stream function, the current updates are calculated by kriging interpolation using the observations and the corresponding model forecast. It is further required that the current updates do not create cross-shore flows; this is represented by the stream function being constant along the coastline and is enforced by incorporating pseudo coastal data into the interpolation. This eliminates the need to construct complex spatial covariance models for the stream function. The method also accommodates observational errors. Results show that the method successfully melds observations into the model, and the influence of data assimilation propagates in space and time.

Citation: Zhang, Z., D. Beletsky, D. J. Schwab, and M. L. Stein (2007), Assimilation of current measurements into a circulation model of Lake Michigan, *Water Resour. Res.*, 43, W11407, doi:10.1029/2006WR005818.

1. Introduction

[2] The North American Great Lakes have been studied extensively both for their scientific value as a large aquatic ecosystem and for their active functions in re-distributing regional water resources and contaminants. Their hydrodynamic behavior is one of the main factors affecting their roles in the regional environment.

[3] Hydrodynamic modeling of currents in the Great Lakes has seen significant progress [Schwab, 1992], with a general trend of improved model accuracy as spatial resolution increases [Beletsky *et al.*, 2006]. In contrast, the accuracy of meteorological forcing functions did not change considerably over the last decade. Since accurate, high-resolution overlake meteorological forecasts are still a somewhat distant prospect, additional improvement in the accuracy of circulation models is likely to be achieved by assimilation of lake-based observational data, especially now, when the Great Lakes Observing System (<http://www.glos.us/>) is being launched.

[4] Data assimilation techniques were pioneered by meteorologists in response to the enormous need for better numerical weather prediction (NWP) [Daley, 1991; Courtier *et al.*, 1993]. They later became widely used by oceanographers [Malanotte-Rizzoli, 1996], and more recently have received applications in other fields of Earth sciences such as

hydrology [McLaughlin, 2002]. Common to these application fields is that the subject is a complex dynamic system whose evolution is typically described by a set of differential equations, which represent physical laws. While modeling these complex systems, one needs to assimilate observations of the state of the system into the model because not only is the model an approximation to the real process, but the initial and boundary conditions can not be perfectly determined. Furthermore, forecast errors tend to magnify with time. By regulating the model state with observations, guided by physical laws that control the behavior of the system, our knowledge of the system state in the form of model forecast is enhanced by the information in the observations whenever they become available. The regulated, or “analyzed”, model state either is provided for applications and decision making, or serves as the now more accurate initial condition for the continued run of the model.

[5] In addition to the analyzed model space, the standard data assimilation scheme also provides a specification of the associated uncertainties in the analyzed fields. These uncertainties, specified in the form of error covariances, are necessarily lower than the uncertainties in the forecast before observations are assimilated (as long as the assimilation is done “right”). The actual amount of this error reduction is related to the error levels in the forecast and in the observation. As the mode steps forward in time, the remaining error in the analysis will deviate the model from its ideal path; in addition, new errors will arise due to deficiencies in the model or uncertainties in external forcings. Keeping track of the evolution of the error covariances is very important for the quality of the assimilation, yet computationally is extremely expensive for large models. Methods for computing the error covariances with improved

¹Center for Integrating Statistical and Environmental Science, University of Chicago, Chicago, Illinois, USA.

²CILER, SNRE, University of Michigan, Ann Arbor, Michigan, USA.

³Great Lakes Environmental Research Laboratory, NOAA, Ann Arbor, Michigan, USA.

⁴Department of Statistics, University of Chicago, Chicago, Illinois, USA.

accuracy at affordable costs continue to be proposed [see, e.g., Evensen, 2003].

[6] Faced with quite different system constraints and much less data than in atmospheric models, data assimilation in oceanic models has had different emphases in approaches and goals. One approach asks the question: “In order to make the model prediction closer to the observations, what should the independent variables (initial conditions, boundary conditions, any external forcing) be?” By subsequently changing the independent variables, the observations are in effect melded into the model. For example, Lynch *et al.* [1998] and He *et al.* [2005] develop an assimilation scheme through such inverse modeling to deduce open-water boundary conditions in the Bay of Maine. Another example is presented by Lewis *et al.* [1998], who create a pseudo shearing stress based on the difference between model-predicted and radar-measured surface velocities, and combine this bogus stress with the observed wind to force the model. A method that has been widely used in oceanic modeling, operationally in some cases, is “optimum interpolation” (OI). In OI, a spatial interpolation of the differences between forecast values and corresponding observations is added to the forecast at each grid point in the model domain. For example, Oke *et al.* [2002] implement an OI procedure to assimilate surface velocity measurements obtained from land-based radar. Because the measurements are on a coarser timescale than the model, and because primitive equation models are sensitive to discontinuous changes to their fields, the data are assimilated gradually in a “time-split” scheme. In assimilating depth-dependent velocity measurements into a 3-D stratified coastal circulation model, Kurapov *et al.* [2005a] use a subset of the moorings for assimilation and the remaining moorings for cross validation. The study shows that impacts of the OI assimilation reach as far as 90 km alongshore. Kurapov *et al.* [2005b] find that velocity data assimilation has a positive impact on other oceanic variables being modeled, such as sea surface height, temperature, potential density, surface salinity, and near-bottom turbulence parameters. In an effort to provide real-time coastal current forecast for vessel traffic agencies, Breivik and Sætra [2001] use high-frequency radar measurements of surface currents in an OI scheme that borrows ideas from ensemble Kalman filter to deal with the error covariance.

[7] This paper presents a method for assimilating current observations into a two-dimensional circulation model of Lake Michigan. The main concerns are to respect the surface level predicted by the model, since we are assimilating *sparse horizontal velocity* observations only, and to ensure that the updated water flow is tangent to the coastline. These requirements provide much-needed constraints on the problem and lead to the key ideas in our solution. The focus is to combine observations and model forecast, subject to the physical constraints mentioned above, to obtain an updated model state that is close to the truth. The performance of this procedure is examined through comparing the original and updated forecasts with independent, validating observations, and through investigating the spatial and temporal persistence of the improvement made by this procedure. The error covariances are

specified subject to some constraints without any formal attempt to estimate them from the available data and model runs. We also note that, although the presented method is a form of OI, we do not strictly use the typical terminology and notation [Ide *et al.*, 1997] in the current literature of atmospheric and oceanic data assimilation.

2. Hydrodynamic Model, Forcing Functions, and Current Meter Data

[8] A two-dimensional barotropic circulation model of Lake Michigan [Beletsky and Schwab, 2001] is used to calculate lake circulation on a regular $2 \text{ km} \times 2 \text{ km}$ horizontal grid. The model is based on the Princeton Ocean Model [Blumberg and Mellor, 1987] and uses nonlinear finite differencing on an Arakawa-C grid with a control volume formalism. The finite differencing scheme is second order and centered in space and time (leapfrog). The model uses time-dependent wind stress forcing at the surface, free-slip lateral boundary conditions, and quadratic bottom friction. The drag coefficient in the bottom friction formulation is 0.0025. The horizontal viscosity coefficient is set to $20 \text{ m}^2/\text{s}$. Previously, the model was successfully applied in this configuration to the Gulf of Riga [Raudsepp *et al.*, 2003].

[9] Hourly meteorological data from 18 stations of the National Weather Service around Lake Michigan and 2 buoys (45002 and 45007) of the National Data Buoy Center (NDBC) are used to generate interpolated, gridded meteorological fields, based on which the momentum fluxes over the water surface at each grid point are calculated. Details of the interpolation and calculations of momentum fluxes are presented by Beletsky and Schwab [2001] and Beletsky *et al.* [2003].

[10] A relatively dense array of 10 current meter moorings was deployed along the southeastern coast of Lake Michigan (Figure 1) in order to measure storm-induced coastal flow. The four central moorings (A1, A2, A4, and A5), deployed in a cluster near a well defined bathymetric feature where topographic steering of coastal flow can be a prominent source of offshore transport, were equipped with Acoustic Doppler Current Profilers (ADCP); the other moorings were equipped with Vector Averaging Current Meters (VACM). The ADCP moorings made measurements at 1 m intervals on the vertical profile from 2 m or 4 m below the surface to 5 m above the bottom. The mid-lake station CM1 made measurements at depths 20 m, 115 m, and 152 m. The other VACM moorings made measurements at 12 m below the surface and 1 m above the bottom. Observations were made from October 1997 to June 1998. We take the depth-averaged, hourly average measurements at each mooring site to make them comparable with the simulated 2-D field.

[11] We test the assimilation method under early spring conditions, when the lake is unstratified and application of a two-dimensional hydrodynamic model is appropriate. Model runs begin on 1 March 1998 and proceed for up to 61 model days. Currents are initialized (for the state at 0000 March 1) using modeled currents from a model run started on 1 January 1998. The model computation uses a 300 s internal time step, each comprising of 30 external time steps. Figure 2 shows the simulation and measurements in the mooring area at hour 80

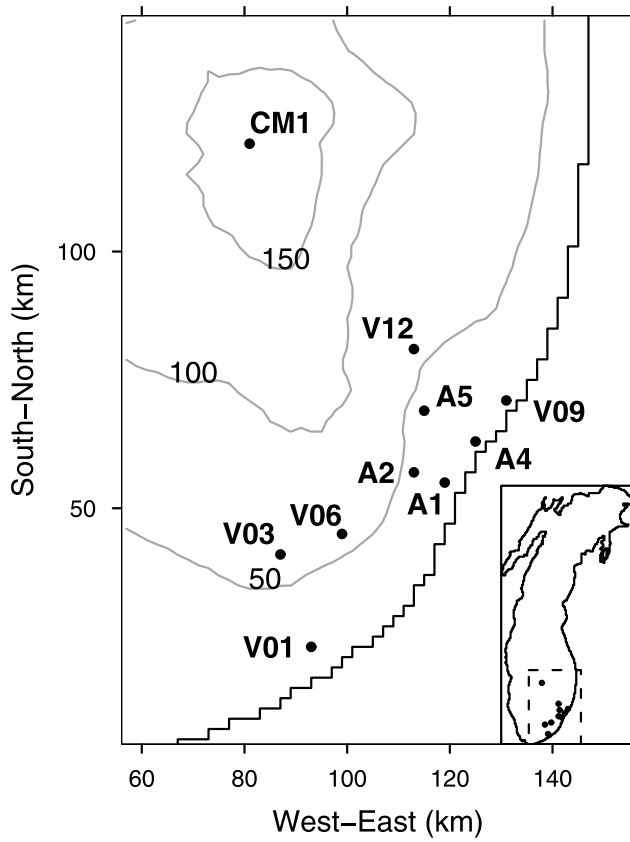


Figure 1. Locations and names of the mooring sites in the south-east portion of Lake Michigan. The contours are water depths in meters. The inset map shows the entire lake and the data area.

(relative to 0000 March 1). It is a typical view of the situation we face in this study.

3. Methodology

[12] For clarity, throughout the work we use bold symbols for vectors. For the components of a vector, we use the corresponding normal-weight symbol with a numeral subscript. For example, if \mathbf{u}^t is the true depth-averaged horizontal velocity, then its east-bound and north-bound components are u_1^t and u_2^t , respectively. In addition, we use subscripts x and y to indicate partial derivatives in the east-bound and north-bound directions.

[13] Let \mathbf{u}^f be the model-forecast depth-averaged horizontal velocity and h the model-forecast water depth, where we omit the superscript on h since we do not update the h field in this study. Similarly, let \mathbf{u}^o be the observation of depth-averaged horizontal velocity. Both \mathbf{u}^f and \mathbf{u}^o are estimates of the true velocity \mathbf{u}^t , which is a function of location and time. Further, let $\Delta = \mathbf{u}^t - \mathbf{u}^f$ be the forecast error. In this study we try to update the model-forecast \mathbf{u}^f by an optimal estimate of Δ , denoted by $\hat{\Delta}$. We are concerned with three constraints.

[14] (1) Physical constraint. Because we have no measurement of surface level, and the distances between the sites of horizontal velocity observations are much greater

than the model grid spacing, we act as if there are no errors in the water depths, so that

$$(h\Delta_1)_x + (h\Delta_2)_y = 0, \quad (1)$$

assuming incompressible water. It is worth emphasizing that the forecast water depth h does change with time; the requirement (1) says that the assimilation does not cause additional change to the model-forecast h .

[15] The relation (1) suggests that Δ can be represented by a stream function, ψ , as

$$\Delta = \left(\frac{1}{h} \psi_y, -\frac{1}{h} \psi_x \right). \quad (2)$$

One can directly verify that the physical constraint (1) is indeed satisfied by $h\Delta$, if the latter is represented as in (2) by an appropriately differentiable scalar field ψ .

[16] (2) Coastal constraint. In our configuration that does not consider tides, there should be no cross-shore water flows, that is, $\mathbf{u}^f + \Delta$ near the coast should be roughly parallel to the coastline. Note that since it is assumed that the forecast velocity itself is parallel to the coast, then so is Δ . This implies that the coastline is a contour of ψ because the contour of the stream function is everywhere tangent to the direction of the vector $h\Delta$. Lacking other mechanisms to ensure that the coastline is indeed a contour of ψ , we simply assign a constant value to ψ along the coast.

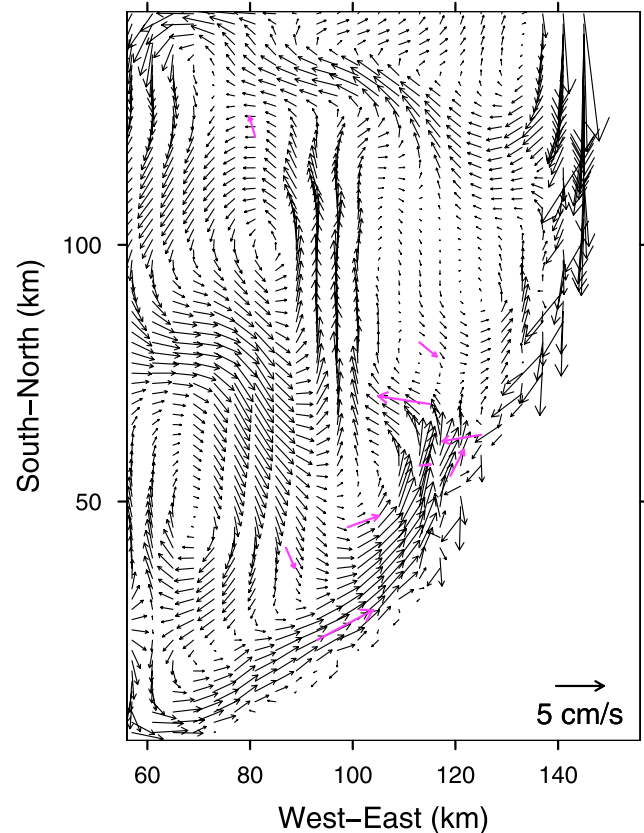


Figure 2. The predicted 2-D velocity field (black arrows) and observations (magenta arrows) at hour 80. At this particular time, measurement at site V09 is missing.

[17] (3) Numerical constraint. Values of $\hat{\Delta}$ at the observational sites are obtainable by comparing the forecast and observed velocities, subject to a certain level of uncertainty. This calls for an interpolation scheme in which the forecast-observation discrepancies contribute to $\hat{\Delta}$ throughout the lake based on the distance between a specific grid point and the observational sites. Naturally, data for this interpolation come from the forecast-observation comparison at the observational sites as well as from our treatment of the coastal constraint.

[18] In summary, the relation (1) provides a basic constraint on the Δ field and leads to the representation of Δ by a stream function ψ . Our approach to modeling ψ is to start out with a simple, mean 0 stationary random process model for it. Given additional information (i.e., constraints (2) and (3)), we estimate Δ via spatial interpolation. The estimation $\hat{\Delta}$ corresponds to the estimation of ψ , which we denote by $\hat{\psi}$. Note, though, that we can directly obtain $\hat{\Delta} = (\frac{1}{h}\hat{\psi}_2, -\frac{1}{h}\hat{\psi}_1)$ and do not need $\hat{\psi}$ itself.

3.1. Observational Data and Pseudo Coastal Data

[19] At an observational site, assume

$$\mathbf{u}^o = \mathbf{u}^f + \boldsymbol{\epsilon}, \quad (3)$$

where $\boldsymbol{\epsilon}$ is an unknown error with zero mean. To simplify the notation later, we combine the forecast and the observation into $\boldsymbol{\xi} \triangleq h(\mathbf{u}^o - \mathbf{u}^f)$. Thus $\boldsymbol{\xi} = h(\Delta + \boldsymbol{\epsilon}) = (\psi_y + h\epsilon_1, -\psi_x + h\epsilon_2)$ and we will use this in estimating Δ .

[20] The following simplifying assumptions are made about the error term $\boldsymbol{\epsilon}$: (1) the error is independent of ψ ; (2) errors at different locations are independent of each other; and (3) the two error components, ϵ_1 and ϵ_2 , are independent of each other. Furthermore, assume the error level is stationary in space, so that $\text{var}(\epsilon_1)$ and $\text{var}(\epsilon_2)$ are each a constant (they do not need to be equal).

[21] We represent the fact that the coastline is a contour of the stream function ψ by creating “pseudo-data” $\psi(\mathbf{p}^c) = 0$ for coastal points \mathbf{p}^c . Because the OI scheme produces spatially continuous updates, if the pseudo data points are sufficiently dense, then $\hat{\psi}$, the estimation of ψ , is kept close to 0 all along the coast. Therefore by conditioning on these pseudo-data, we ensure that the stream function is effectively constant along the coast.

[22] Now, if we have n observational sites ($n \leq 10$ in the present setting, noticing that we may choose to use only part of the available observations) and have chosen m coastal pseudo data points, then our data vector is

$$\mathbf{z} = [\xi_1(\mathbf{p}_1^o), \dots, \xi_1(\mathbf{p}_n^o), \xi_2(\mathbf{p}_1^o), \dots, \xi_2(\mathbf{p}_n^o), \psi(\mathbf{p}_1^c), \dots, \psi(\mathbf{p}_m^c)]^T. \quad (4)$$

This data vector contains information about ψ , ψ_x , ψ_y , $\boldsymbol{\epsilon}$, and h . The data $\xi_1(\mathbf{p}^o)$ and $\xi_2(\mathbf{p}^o)$ serve to steer the forecast velocity at location \mathbf{p}^o to be close to the observation. The zero-valued pseudo-data $\psi(\mathbf{p}^c)$ serve to maintain parallel-to-the-coast velocities along the coast.

3.2. The Dual Kriging Interpolation Method

[23] Using the data \mathbf{z} , we obtain the velocity update $\hat{\Delta}$ at each model grid by kriging interpolation, which is “opti-

mal” in the sense that it gives the best linear unbiased estimation [Stein, 1999] under the assumed covariances between the variables involved (see Section 3.4). Here, “best” means the variance of estimation error is minimized. The dual simple kriging (dSK) algorithm [Goovaerts, 1997, p. 169–173] formulates $\hat{\Delta}_1$, the estimate of Δ_1 (i.e., the forecast error of the velocity component u_1) at location \mathbf{p} , as a linear combination of the covariances between the unknown and the data:

$$\hat{\Delta}_1(\mathbf{p}) = \mathbf{k}^T \boldsymbol{\lambda}, \quad (5)$$

where $\mathbf{k} = \text{cov}(\Delta_1(\mathbf{p}), \mathbf{z})$ is the unknown-to-data covariance vector and $\boldsymbol{\lambda}$ are the dual weights, or interpolation coefficients. Let $\mathbf{K} = \text{cov}(\mathbf{z}, \mathbf{z})$ be the data-to-data covariance matrix, then the dual weights are given by [Goovaerts, 1997, p. 169]

$$\boldsymbol{\lambda} = \mathbf{K}^{-1} \mathbf{z}. \quad (6)$$

The update to the u_2 component, $\hat{\Delta}_2$, is estimated separately in a similar procedure.

[24] According to (6), the dual weights are dependent on the covariance model and the data (both locations and values) but are independent of the location \mathbf{p} at which Δ is sought. Therefore for fixed \mathbf{z} and \mathbf{K} , one needs to solve for $\boldsymbol{\lambda}$ only once. This is a main advantage of using dSK over SK, which requires recalculation of the interpolation coefficients for different \mathbf{p} .

3.3. Derivations With a Spatially Stationary Covariance Function for ψ

[25] In order to carry out this interpolation, one needs to compute the covariances \mathbf{k} and \mathbf{K} . Assume the covariance function of ψ is stationary in space, and use the following notation for the covariance between two locations \mathbf{p}_1 and \mathbf{p}_2 :

$$\text{cov}(\psi(\mathbf{p}_1), \psi(\mathbf{p}_2)) \triangleq \varphi(\boldsymbol{\ell}), \quad \text{where } \boldsymbol{\ell} = \mathbf{p}_2 - \mathbf{p}_1.$$

This notation allows for geometric anisotropy in the covariance structure, although anisotropy will not be explored in this study. The following basic relations will be used in calculating the data-to-data and unknown-to-data covariances:

$$\begin{aligned} \text{cov}(\psi(\mathbf{p}_1), \psi_x(\mathbf{p}_2)) &= \varphi_x(\mathbf{p}_2 - \mathbf{p}_1) \\ \text{cov}(\psi(\mathbf{p}_1), \psi_y(\mathbf{p}_2)) &= \varphi_y(\mathbf{p}_2 - \mathbf{p}_1) \\ \text{cov}(\psi_x(\mathbf{p}_1), \psi_x(\mathbf{p}_2)) &= -\varphi_{xx}(\mathbf{p}_2 - \mathbf{p}_1) \\ \text{cov}(\psi_y(\mathbf{p}_1), \psi_y(\mathbf{p}_2)) &= -\varphi_{yy}(\mathbf{p}_2 - \mathbf{p}_1) \\ \text{cov}(\psi_x(\mathbf{p}_1), \psi_y(\mathbf{p}_2)) &= -\varphi_{xy}(\mathbf{p}_2 - \mathbf{p}_1) \\ \text{cov}(\psi_y(\mathbf{p}_1), \psi_x(\mathbf{p}_2)) &= -\varphi_{yx}(\mathbf{p}_2 - \mathbf{p}_1) \end{aligned} \quad (7)$$

(Because φ_x and φ_y will be odd functions about the origin, the direction of their vector arguments is significant.)

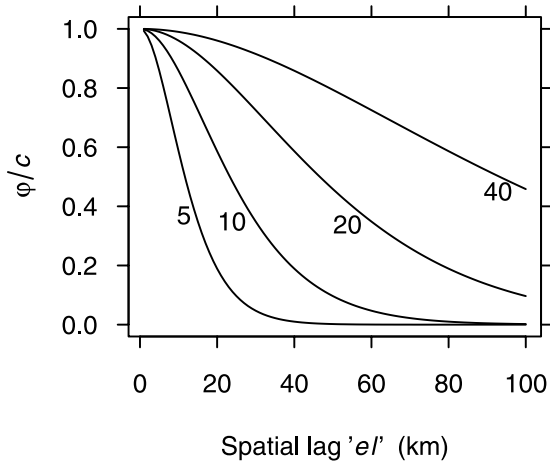


Figure 3. The covariance function $\phi(\ell)$, defined in (10), with several values for the range α : 5 km, 10 km, 20 km, and 40 km. The abscissa is the spatial lag ℓ in (10); the ordinate is ϕ normalized by c , i.e., $\phi(0)$.

[26] With the simplifying assumptions about the observation error ϵ , the elements of the data-to-data covariance matrix \mathbf{K} are

$$\begin{aligned} \text{cov}(\xi_1(\mathbf{p}_1), \xi_1(\mathbf{p}_2)) &= -\phi_{yy}(\mathbf{p}_2 - \mathbf{p}_1) + \mathbb{I}_{\mathbf{p}_1=\mathbf{p}_2} h^2(\mathbf{p}_1) \text{var}(\epsilon_1) \\ \text{cov}(\xi_1(\mathbf{p}_1), \xi_2(\mathbf{p}_2)) &= \phi_{xy}(\mathbf{p}_2 - \mathbf{p}_1) \\ \text{cov}(\xi_2(\mathbf{p}_1), \xi_2(\mathbf{p}_2)) &= -\phi_{xx}(\mathbf{p}_2 - \mathbf{p}_1) + \mathbb{I}_{\mathbf{p}_1=\mathbf{p}_2} h^2(\mathbf{p}_1) \text{var}(\epsilon_2) \\ \text{cov}(\psi(\mathbf{p}_1), \xi_1(\mathbf{p}_2)) &= \phi_y(\mathbf{p}_2 - \mathbf{p}_1) \\ \text{cov}(\psi(\mathbf{p}_1), \xi_2(\mathbf{p}_2)) &= -\phi_x(\mathbf{p}_2 - \mathbf{p}_1) \\ \text{cov}(\psi(\mathbf{p}_1), \psi(\mathbf{p}_2)) &= \phi(\mathbf{p}_2 - \mathbf{p}_1) \end{aligned} \quad (8)$$

where \mathbf{p}_1 and \mathbf{p}_2 are the locations of two (actual or pseudo) data points. The symbol \mathbb{I} is the identity operator: $\mathbb{I}_{\mathbf{p}_1=\mathbf{p}_2}$ is 1 if locations \mathbf{p}_1 and \mathbf{p}_2 coincide, and 0 otherwise.

[27] The elements of the unknown-to-data covariance vector \mathbf{k} are

$$\begin{aligned} \text{cov}(\Delta_1(\mathbf{p}), \xi_1(\mathbf{p}')) &= -\frac{1}{h(\mathbf{p})} \phi_{yy}(\mathbf{p}' - \mathbf{p}) \\ \text{cov}(\Delta_1(\mathbf{p}), \xi_2(\mathbf{p}')) &= \frac{1}{h(\mathbf{p})} \phi_{xy}(\mathbf{p}' - \mathbf{p}) \\ \text{cov}(\Delta_1(\mathbf{p}), \psi(\mathbf{p}')) &= \frac{1}{h(\mathbf{p})} \phi_y(\mathbf{p}' - \mathbf{p}) \\ \text{cov}(\Delta_2(\mathbf{p}), \xi_1(\mathbf{p}')) &= \frac{1}{h(\mathbf{p})} \phi_{xy}(\mathbf{p}' - \mathbf{p}) \\ \text{cov}(\Delta_2(\mathbf{p}), \xi_2(\mathbf{p}')) &= -\frac{1}{h(\mathbf{p})} \phi_{xx}(\mathbf{p}' - \mathbf{p}) \\ \text{cov}(\Delta_2(\mathbf{p}), \psi(\mathbf{p}')) &= -\frac{1}{h(\mathbf{p})} \phi_x(\mathbf{p}' - \mathbf{p}) \end{aligned} \quad (9)$$

where \mathbf{p} is any model grid point and \mathbf{p}' is a (pseudo or actual) data point.

[28] Note that, due to the independence assumptions on the error terms, the observation errors ϵ only affect the diagonal elements of the matrix \mathbf{K} and does not affect the vector \mathbf{k} .

3.4. A Parametric Model for the Covariance of ψ

[29] As is evident in (8) and (9), the covariance structure of the stream function, $\phi(\ell)$, is key to calculating \mathbf{k} and \mathbf{K} , which are essential information for the kriging interpolation. One may either take a parametric form for $\phi(\ell)$ or seek it by empirical means. For explorations, we use an isotropic model of the following form for the covariance at spatial lag $\ell = (\ell_1, \ell_2)$:

$$\phi(\ell) = \phi(\ell) = ce^{-\ell/\alpha} (1 + \ell/\alpha + \ell^2/(3\alpha^2)), \quad (10)$$

where $\ell = \sqrt{\ell_1^2 + \ell_2^2}$ and $c = \phi(0)$, i.e., the variance of ψ . The parameter α will be called the “range” of the model. Larger values of α correspond to covariance structures with longer correlation ranges. Figure 3 shows this covariance function with α taking several values. This covariance function corresponds to a process ψ that is exactly two times differentiable (in the mean square sense, see *Stein* [1999, p. 28]). As a result, in addition to Δ being expressible in terms of the first derivatives of ψ , Δ itself is also differentiable. We choose not to use a covariance model that corresponds to a process with many more derivatives because such models sometimes produce interpolations with unrealistic properties [*Stein*, 1999, p. 211–223].

[30] The derivatives of $\phi(\ell)$ that are needed in (8) and (9) are

$$\begin{aligned} \phi_x(\ell) &= -ce^{-\ell/\alpha} \ell_1 (1 + \ell/\alpha) / (3\alpha^2) \\ \phi_y(\ell) &= -ce^{-\ell/\alpha} \ell_2 (1 + \ell/\alpha) / (3\alpha^2) \\ \phi_{xx}(\ell) &= -ce^{-\ell/\alpha} (1 + \ell/\alpha - \ell_1^2/\alpha^2) / (3\alpha^2) \\ \phi_{yy}(\ell) &= -ce^{-\ell/\alpha} (1 + \ell/\alpha - \ell_2^2/\alpha^2) / (3\alpha^2) \\ \phi_{xy}(\ell) &= ce^{-\ell/\alpha} \ell_1 \ell_2 / (3\alpha^4) \end{aligned} \quad (11)$$

[31] Note that if there is no observation error, i.e., $\epsilon \equiv 0$ in (3) and hence $\text{var}(\epsilon_1) = \text{var}(\epsilon_2) = 0$ in (8), then the variance c will cancel in the interpolation (see (5), (6), (8), (9) and (11) collectively). In this case, α is the only parameter in the covariance model that needs to be estimated. We take an empirical approach to its estimation: leave out certain observational sites, assimilate the observations at the other sites using a series of α values, and choose the α value with which the updated velocities at the unused sites are close to their observations. This procedure is discussed in detail in the next section after a measure is defined for the “closeness” of two velocities.

[32] We have found that including observation errors at the levels we estimated has only a small influence on the result of the assimilation. Therefore all the results presented below ignore observation errors. Consequently, the parameter c does not need to be estimated.

4. Results and Discussion

[33] We show results using the parametric covariance model proposed in Section 3.4. The assimilation procedure is outlined as follows:

[34] 0. Estimate the parameter α in the covariance model.

[35] 1. Obtain the forecast and the corresponding observations for the model time.

[36] 2. Calculate the data \mathbf{z} (def. 4).

[37] 3. Calculate the data-to-data covariance matrix \mathbf{K} (Equations 8 and 11).

[38] 4. Calculate the interpolation coefficients λ (Equation (6)).

[39] 5. For each model grid, calculate the unknown-to-data covariance vector \mathbf{k} ((9) and (11)), then obtain the velocity component updates Δ_1 and Δ_2 (Equation (5)), and finally update the forecast \mathbf{u}^f with $\mathbf{u}^f + \Delta$.

[40] 6. Run the hydrodynamic model until the next observation time, then repeat steps 1–6.

[41] The observations and model output are comparable hourly averages. Some results shown below are “snapshot” assimilations of observations into model output of the corresponding hour. This static processing after the model run has finished provides diagnostics of assimilation conducted with forecast and observation on the same timescale (both being hourly averages). When assimilation is performed “continuously” as the model runs, observations of hour i are assimilated after the internal step (see Section 2) that is closest to the time $(i - 0.5)$ hour; therefore exactly one assimilation is conducted in an hour. In this dynamic process, the forecast represents the average model state in a 300 s internal step; therefore it is not exactly comparable with the hourly time-average observations. However, we were unable to obtain instantaneous measurements for this study. Also contributing to the uncertainties is the different spatial resolution of the model output and the observations: the former are model-grid averages and the latter are point-wise.

4.1. A Measure of Vector Similarity

[42] As a tool to be used in the following sections, we define a measure of the similarity between two velocities \mathbf{u}_1 and \mathbf{u}_2 as

$$\rho = 1 - \frac{\|\mathbf{u}_1 - \mathbf{u}_2\|}{b + \max(\|\mathbf{u}_1\|, \|\mathbf{u}_2\|)}, \quad (12)$$

where the empirically-determined parameter b , $b > 0$, maintains continuity of ρ at $\max(\|\mathbf{u}_1\|, \|\mathbf{u}_2\|) = 0$ and downweights pairs of unusually small \mathbf{u} 's (so that a pair of small velocities produce a large ρ , regardless of the actual values of those two small velocities). The value of b taken here is the 10th percentile of the observed speeds at all the mooring sites. This measure has some properties that are desirable in this study:

[43] (a) The value of ρ lies between -1 and 1 , is close to -1 when $\mathbf{u}_1 = -\mathbf{u}_2$ with both vectors reasonably large, is equal to 1 when $\mathbf{u}_1 = \mathbf{u}_2$, and is also close to 1 if both vectors are notably small compared to b .

[44] (b) When the angle between \mathbf{u}_1 and \mathbf{u}_2 is fixed, the value of ρ tends to 0 as $\max(\|\mathbf{u}_1\|, \|\mathbf{u}_2\|)/\min(\|\mathbf{u}_1\|, \|\mathbf{u}_2\|)$ increases.

[45] (c) When the magnitudes of \mathbf{u}_1 and \mathbf{u}_2 are fixed, the value of ρ increases as their directions become closer.

[46] Measures of similarity and dissimilarity for scalar and vector variables are discussed by *Gentle* [2002, p. 109–122]. However, none of the measures on his list for vector variables has all the three properties (a)–(c). Particularly, vectors are often compared using distance-type measures.

Compared to the ρ defined above, distance-type measures have two drawbacks. First, they are defined to be non-negative and hence lack indications that two vectors can be opposite in directions. Second, they typically are not scaled to a fixed range, e.g., $[0, 1]$; this makes it difficult to appreciate the magnitude of a specific value of the measure. *Schwab* [1983] defines a “Fourier norm” (also used by *Beletsky et al.* [2003, 2006]) for similar purposes. In contrast to ρ , which aims for the comparison of two vector values, the Fourier norm is designed to yield a single measure for the comparison of two paired vector series. In addition to vector distances, some vector correlations have been proposed [*Hanson et al.*, 1992]. However, as correlations, they are unaffected by linear transformations of either variable, and therefore do not suit the need of this study. A still common practice in comparing two vector series is to examine the vector components separately [see *Davies et al.*, 2001; *Oke et al.*, 2002; *Beletsky et al.*, 2003; *Kurapov et al.*, 2005a].

4.2. Estimation of the Range Parameter of the Covariance Model

[47] As noted already, we only consider the case in which observation errors are ignored, so that the range α is the only parameter that needs to be estimated for the covariance model (c is set to 1 because it cancels). We estimate α using a cross-validation procedure [*Wahba et al.*, 1995] based on a reference model run for the first 59 days of 1998, so that the testing period (days 60 to 120) used in all subsequent subsections where the estimated α value will be used is different from the fitting period. Here a “reference” model run is a model run with no data assimilation; its velocity prediction will be denoted by \mathbf{u}^f .

[48] We conducted a series of snapshot assimilations on hourly average model predictions produced by the reference model run. At a particular model hour i , we left out the j -th observational site (j is one of $1, \dots, 10$) and assimilated the observations at all the other sites using values 2 km, 4 km, \dots , 30 km for α . In this fashion, each observational site was left out in turn. This procedure was repeated for model hours $i = 10, 40, 70, \dots, 1390$.

[49] After each assimilation, which corresponds to a particular (i, j, α) combination, we examine the change to the model-observation agreement at site j caused by the assimilation, and quantify this change by

$$D_a(\alpha, j, i) = \rho(\mathbf{u}^r + \hat{\Delta}, \mathbf{u}^o) - \rho(\mathbf{u}^f, \mathbf{u}^o). \quad (13)$$

The two ρ 's on the right-hand side are the analysis-observation and forecast-observation vector similarities for observational site j and model hour i , using the specific α value in the covariance function. A larger positive D_a suggests greater improvement to the model forecast at site j .

[50] Figure 4 shows D_a , averaged over all the tested model hours i for each observational site and α value. For most sites, the pattern is clear that the assimilation performs better as α increases until it reaches an optimal value around 10 km, after which the performance decreases. Despite this similar pattern, the overall level of D_a differs greatly between the sites. For example, with any particular α value, the assimilation usually has the most positive influence at sites A2, V03, and V06, followed by A4, but has the worst

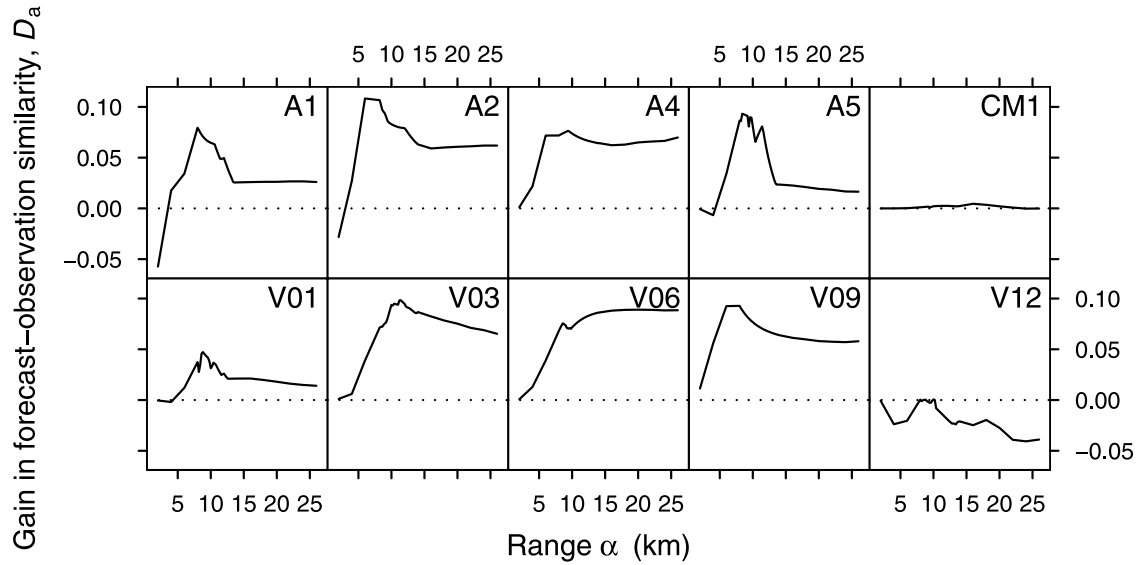


Figure 4. The (non-dimensional) gain in the velocity similarity, D_a , defined in (13), caused by data assimilation. Here D_a is plotted as a function of the range parameter α . In each panel, the particular site being plotted is left out while all other sites are used in the assimilation.

influence at site V12, where D_a is mostly negative. It is not surprising so see that the mid-lake site CM1 only starts to be slightly affected by assimilating the observations at the other sites when α exceeds 10 km, which is when the site CM1 starts to have appreciable correlation with at least one other observational site. The site CM1 can demonstrate greater impact of the assimilation if the range α is beyond the largest value shown. However, such an α value would be too large for the other sites. Perhaps more interesting is that site V12 is harmed by the assimilation of observations at the other sites. This may suggest that the chosen covariance model is not suitable for the region of V12. One certainly can not expect the proposed covariance model, or any stationary and isotropic model, to be appropriate for a large region in the lake, even with the use of pseudo coastal data. Nonetheless, the consistent pattern shown by most sites in Figure 4 is support for this method of estimating α .

[51] Averaging D_a over not only i but also j gives rise to a single curve of D_a as a function of α that suggests 12.0 km is the optimal value for α , as shown in Figure 5. Figure 5 also reveals that we actually took denser samples of α around 10 km after we had learned that the optimal α is close to that value.

[52] Figure 6 shows the updated velocity field by a snapshot assimilation for model hour 80, using the estimated range parameter $\hat{\alpha} = 12.0$ km, ignoring observation errors and using 100 coastal pseudo data points. This is the typical parameterization used to create most demonstrations from this point on. A comparison of Figure 6 with Figure 2 shows how the forecast velocity field is modified by the assimilation of observations. Particularly, the updated velocities at the observational sites agree with their corresponding observations because the latter has been assumed error-free in the assimilation. Moreover, the velocity field in the neighborhood of each observational site is modified more or less smoothly.

4.3. Impact of the Coastal Pseudo Data Points

[53] Recall that, to prevent the assimilation from generating cross-shore velocity components, we create pseudo data points along the coast with value $\psi = 0$ to help maintain that the estimation $\hat{\psi}$ is constant along the coast. These pseudo-data are used in the interpolation so that they exert a “stabilizing” force in their neighborhoods. On the basis of experimentations, we have fixed the number of coastal points at 100. These points are chosen with a preference to the coastal stretches close to the mooring sites. The role of these pseudo-data is clear upon comparing Figure 6 with Figure 7, which is the result of a snapshot assimilation

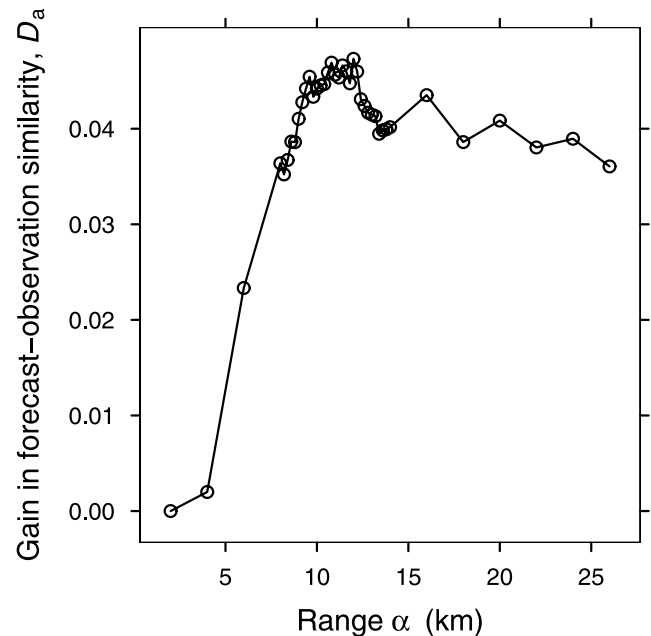


Figure 5. The curves in Figure 4 averaged over the observational sites for each α value.

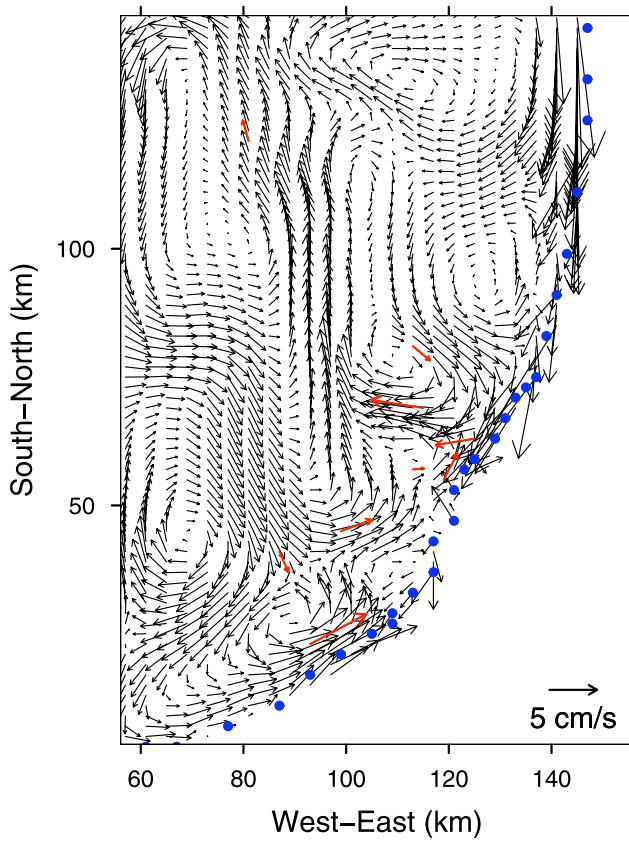


Figure 6. The analyzed (or updated) velocity field, $\mathbf{u}^f + \Delta$, by a snapshot assimilation for hour 80, using 100 coastal pseudo data points (blue dots). The range parameter α is 12.0 km. The red arrows are observations that have been assimilated. Compare with Figure 2.

without these pseudo-data. The discretization of the model domain into square grid boxes makes both the coastline and this treatment only approximate.

4.4. Spatial and Temporal Propagation of the Assimilation Effect

[54] Through spatial interpolation, the assimilation of observations at a small number of locations affects the velocities at other locations. Moreover, the assimilation influences the future development of the model through an updated velocity field at the present time. To quantitatively examine these spatial and temporal effects, we conducted 140 assimilation experiments, each starting at one of 140 different times. For each experiment, we first ran the hydrodynamic model to its starting time, without assimilating any observations. Then in the next 10 h, observations at 9 sites were assimilated, leaving out the observations at a particular site j . After this 10-h assimilation, the model continued for 24 h without further assimilation. Since each experiment used 9 of the 10 observational sites, each site was left out in 14 of these 140 experiments and was assimilated in the other 126 experiments.

[55] In any such experiment, we measure the model performance at site j in hour $i = 0, \dots, 24$ after the assimilation period by

$$D_f(j, i) = \rho(\mathbf{u}^f, \mathbf{u}^o) - \rho(\mathbf{u}^r, \mathbf{u}^o), \quad (14)$$

where \mathbf{u}^f is the hourly average prediction (forecast) in the assimilated model run, and \mathbf{u}^r is the corresponding prediction in a reference model run. The two ρ 's on the right-hand side are the prediction-observation similarities, in the assimilated and reference model runs respectively, for site j in hour i after the end of the assimilation period. Clearly, D_f indicates the (positive or negative) impact of the assimilation on the model prediction at site j after the assimilation. The D_f are averaged for each data site j in the assimilating (or leaving-out) role over the 126 (or 14) experiments; the averages are shown in Figure 8. It can be seen that, for up to a day after the 10-h assimilation, the model predictions at an assimilated observational site remain closer to the observations compared to the reference model run. At a site that has been left out in the preceding assimilation, the model performance shows varied patterns. First of all, the mid-lake site CM1 shows little impact by assimilating observations at the other sites, apparently because the distance between the mid-lake site and the assimilated sites is large compared with the correlation range of the covariance model. The sites A4, V03, V09, and V12 have benefited during the assimilation period, as can be seen in hour 0, and the benefit remains visible for up to half a day after the assimilation. Interestingly, the (positive or negative) impact of assimilation on an unassimilated site may have a time lag, most notably at the site V12. These patterns of the assimilation effect at unassimilated sites are influenced by the covariance model used.

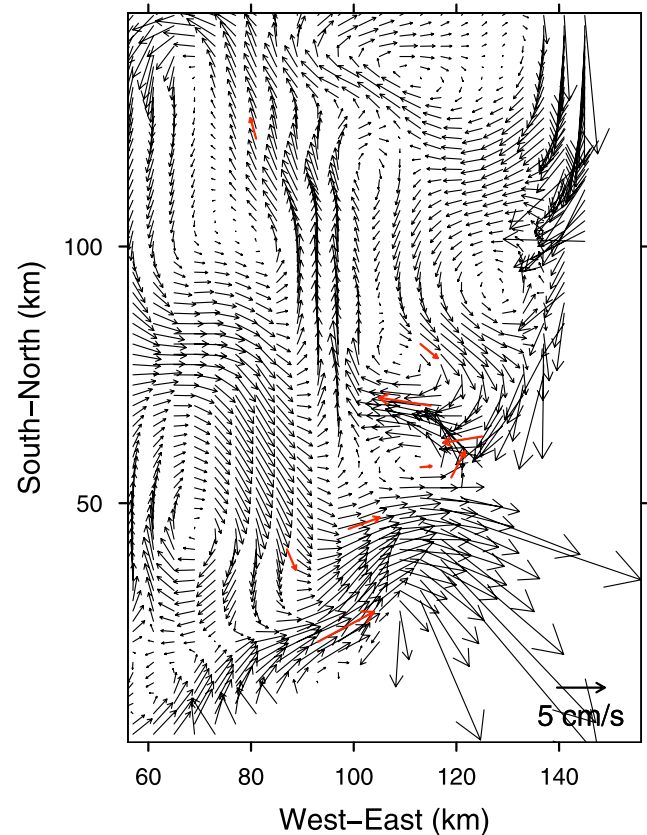


Figure 7. The analyzed (or updated) velocity field for hour 80 in the same setting as Figure 6 except that no coastal pseudo data point is used.

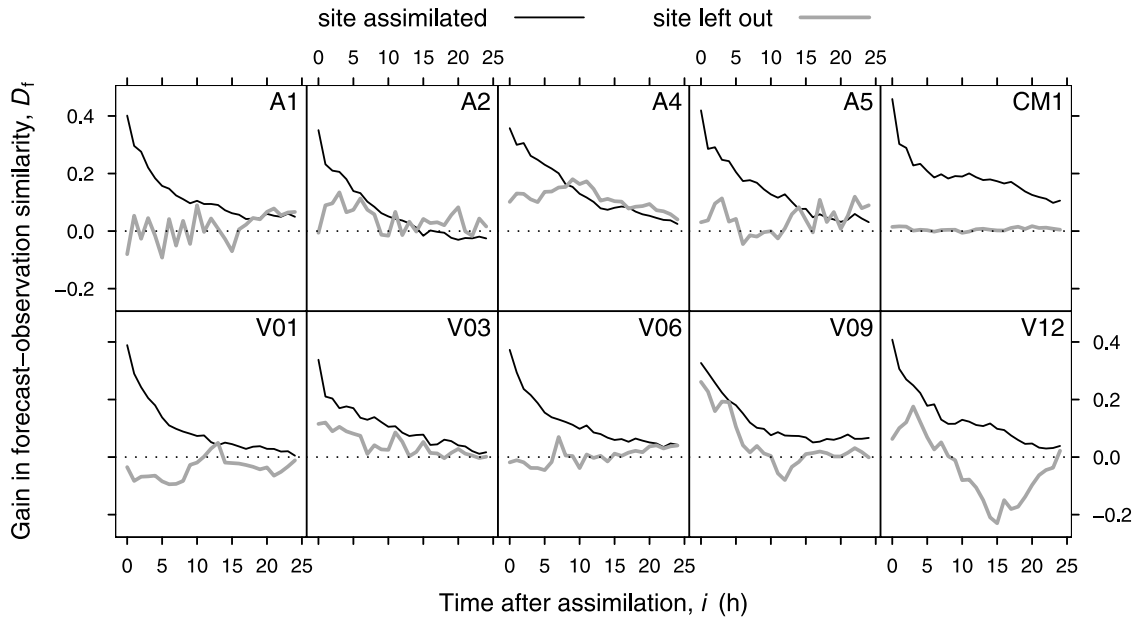


Figure 8. The (non-dimensional) gain in the prediction-observation similarity, $D_f^f(j, i)$, defined in (14), induced by assimilating observations into the model. For each observational site j , D_f is plotted as a function of the time i after the assimilation period. The assimilations leave out one site and use the observations of all other sites. The black curve is the case where the site in question is assimilated; the gray curve is the case where the site is left out (but is affected by the assimilation of other sites).

[56] Although there are only 10 observational sites at which the *improvement* made by assimilation can be examined, the *change* caused by assimilation can be examined throughout the lake by comparing the velocity fields in model runs with and without assimilation. In each of the 140 assimilation experiments, we take the velocity fields at 0 and 24 h after the end of the assimilation period and calculate their similarities (defined in (12)) at each grid point with the corresponding fields in the reference model run. Figure 9 shows these two images of velocity similarity, averaged over the 140 experiments. Lower similarities indicate bigger changes caused by the assimilation. The right panel of Figure 9 suggests that it is difficult for the model to completely “wash out” the influence of the 10-h assimilation and return to a state that looks as though the velocity forecast had never been modified by data assimilation. In addition, in Figure 9 we notice the following patterns:

[57] 1. The assimilation has a high impact around the assimilated observational sites. There are also high-impact regions, e.g., around “X” and “Y”, that are not particularly close to the observational sites. The strong assimilation effect in these regions arises from the interactions between the covariance model, the actual flow pattern in the entire southeast portion of the lake, and the comparison between the forecast and observed velocities at the mooring sites.

[58] 2. Where there is a cluster of assimilated observational sites (e.g., {A1, A2, A4, A5, V09} or {V03, V06}), the assimilation can have a strong impact over a continuous region covering the sites.

[59] 3. At the mid-lake site CM1, the impact of the assimilation extends in a more or less circular fashion, consistent with the isotropic covariance function used. Because of the lack of neighboring observational sites and the distance to the coast, it appears the impact of

assimilating CM1 is spatially less restricted than that of the other observational sites.

[60] 4. The impact of the assimilation extends far into the area marked by “Z”. This effect may have close relations with the dominant northerly flow patterns in that area [Beletsky *et al.*, 1999].

5. Summary

[61] The key to the proposed method is the formulation of the depth constraint (Equation (1)) and its representation via the stream function (expression (2)). The formulation (1) translates the fact that we do not know the true water depth to the constraint that our modification to the horizontal velocity should not suggest any particular error in the model-predicted water depth. This formulation establishes a connection between the velocity updates at neighboring grids and beyond (the formulation is actually in continuous space). More importantly, the formulation (1) leads to the representation (2), which strategically links the vector field Δ , the physical constraint (1) on this vector field, and the stream function ψ , which is a scalar field. When we work on the stream function under mild differentiability requirements, we are working on the two components of Δ simultaneously with the physical constraint (1) satisfied.

[62] The stream function representation also leads naturally to our treatment of the coastal constraint. The pseudo coastal data easily integrates into the interpolation framework. The number and locations of the pseudo data points to be created are fully controlled by us. We place more of them close to the observational sites, and determine their number so that enough control is exerted along the coast in the results of the interpolation. This treatment translates a tricky relation, i.e., the vector Δ is parallel to the coastline,

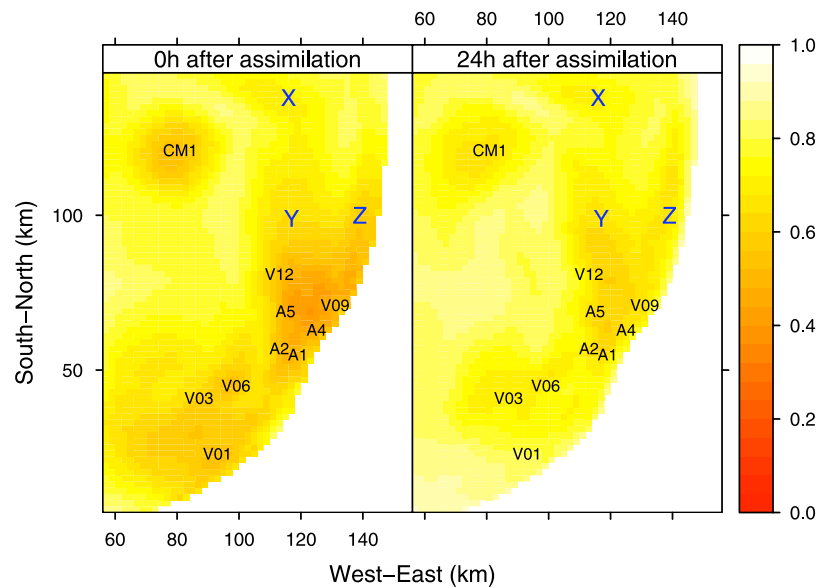


Figure 9. The vector similarity ρ , defined in (12), between velocity fields at corresponding times predicted by assimilated and reference model runs. The left panel is at the end of the 10-h assimilation period; the right is 24 h after the assimilation period. Lower ρ values suggest larger impact by the assimilation. The letters “X”, “Y”, and “Z” mark several regions not particularly close to the observational sites but showing high impact of assimilation; these regions are discussed in the text.

to a simple assignment, i.e., ψ takes a particular value at selected locations.

[63] The coastal pseudo-data have a more subtle role. Because the stream function ψ is constant along the coast, its covariance between an in-lake point and a coastal point is zero. This implies that the spatial covariance structure of ψ is nonstationary and anisotropic, because different in-lake points have different spatial relationships with the coast. However, this is in conflict with our (rather desirable) choice to describe the covariance of ψ with a stationary, isotropic model. Fortunately, after introducing the pseudo coastal data, the actual covariance of ψ is the assumed stationary, isotropic model conditional on the pseudo-data. This conditional covariance model, which is effectively used in the kriging interpolation, is nonstationary and anisotropic, only not explicitly written out. The pseudo coastal data “guide” the interpolation near the coast and eliminate the need to construct directly such complex covariance models.

[64] We have used a stationary, isotropic covariance function with a parametric form (defined in (10)) to illustrate the method, and have shown that largely positive influences of the data assimilation propagate spatially from the observational sites and temporally to as far as a day in the future. More elaborate quantification of the method’s performance is hindered by the quality of the data. Of the 10 mooring sites, the 4 ADCP sites each has measurements at 14 to 34 depths, whereas the 6 VACM sites have measurements at 2 or 3 depths only (see Section 2). Depth-averaged measurements at these sites obviously have different levels of precision. The proposed method has provisions for observation errors (see (3) and (8)), although we have focused on presenting results that ignore these errors.

[65] Typical data assimilation work includes another error component—the forecast error, characterized by its covariance matrix, which may evolve with time. In the proposed method, the covariance structure of the forecast error is contained in the covariance model of the stream function, i.e., $\phi(\ell)$ as defined in (10). The temporal evolution of $\phi(\ell)$ is the subject of future work.

[66] Given the active role of the Great Lakes as a vehicle for transporting and dispersing sediments and pollutants, the ability to accurately predict the velocity field has obvious bearings on environmental studies of these water bodies. Stroud *et al.* [2006] describe a data assimilation method using satellite images and the circulation model we have used in this study to predict sediment transport in southern Lake Michigan. In a sense, the modeling of currents is a topic upstream of that of sediment transport. Collaborations are underway to connect the data assimilation of velocity fields, described here, with the modeling of sediment transport. One can also imagine going further upstream by using the results of this study to inform about errors in the forcing wind field, which is derived by interpolating mostly land-based observations and therefore involves considerable uncertainty.

[67] **Acknowledgments.** The authors thank the reviewers and the editors for their very constructive comments. This is GLERL Contribution No. 1441. Although the research described in this article has been funded wholly or in part by the United States Environmental Protection Agency through STAR Cooperative Agreement #R-82940201-0 to the University of Chicago, it has not been subjected to the Agency’s required peer and policy review and therefore does not necessarily reflect the views of the Agency, and no official endorsement should be inferred.

References

- Beletsky, D., and D. J. Schwab (2001), Modeling circulation and thermal structure in Lake Michigan: Annual cycle and interannual variability, *J. Geophys. Res.*, 106(C9), 19,745–19,771.

- Beletsky, D., J. H. Saylor, and D. J. Schwab (1999), Mean circulation in the Great Lakes, *J. Great Lakes Res.*, 25(1), 78–93.
- Beletsky, D., D. J. Schwab, P. J. Roebber, M. J. McCormick, G. S. Miller, and J. H. Saylor (2003), Modeling wind-driven circulation during the March 1998 sediment resuspension event in Lake Michigan, *J. Geophys. Res.*, 108(C2), 3038, doi:10.1029/2001JC001159.
- Beletsky, D., D. J. Schwab, and M. J. McCormick (2006), Modeling 1998–2003 summer circulation and thermal structure in Lake Michigan, *J. Geophys. Res.*, 111, C10010, doi:10.1029/2005JC003222.
- Blumberg, A. F., and G. L. Mellor (1987), A description of A three-dimensional coastal ocean circulation model, in *Three-Dimensional Coastal Ocean Models, Coastal Estuarine Science*, vol. 5, edited by N. S. Heaps, pp. 1–16, AGU, Washington D. C.
- Breivik, Ø., and Ø. Sætra (2001), Real time assimilation of HF radar currents into a coastal ocean model, *J. Mar. Syst.*, 28, 161–182.
- Courtier, P., J. Derber, R. Errico, J.-F. Louis, and T. Vukićević (1993), Important literature on the use of adjoint, variational methods and the Kalman filter in meteorology, *Tellus Ser. A: Dyn. Meteorol. Oceanogr.*, 45, 342–357, doi:10.1034/j.1600-0870.1993.t01-4-00002.xPDF.
- Daley, R. (1991), *Atmospheric Data Analysis*, Cambridge Univ. Press, Cambridge.
- Davies, A. M., P. Hall, M. J. Howarth, P. Knight, and R. Player (2001), A detailed comparison of measured and modeled wind-driven currents in the North Channel of the Irish Sea, *J. Geophys. Res.*, 106(C9), 19,683–19,713.
- Evensen, G. (2003), The Ensemble Kalman Filter: Theoretical formulation and practical implementation, *Ocean Dyn.*, 53, 343–367, doi:10.1007/s10236-003-0036-9.
- Gentle, J. E. (2002), *Elements of Computational Statistics*, Springer.
- Goovaerts, P. (1997), *Geostatistics for Natural Resources Evaluation*, Applied Geostatistics Series, Oxford Univ. Press, New York.
- Hanson, B., K. Klink, K. Matsuura, S. M. Robeson, and C. J. Sillmott (1992), Vector correlation: Review, exposition, and geographic application, *Ann. Assoc. Am. Geogr.*, 82(1), 103–116.
- He, R., D. J. McGillicuddy, D. R. Lynch, K. W. Smith, C. A. Stock, and J. P. Manning (2005), Data assimilative hindcast of the Gulf of Maine coastal circulation, *J. Geophys. Res.*, 110, C10011, doi:10.1029/2004JC002807.
- Ide, K., P. Courtier, M. Ghil, and A. C. Lorenc (1997), Unified notation for data assimilation: Operational, sequential and variational, *J. Meteorol. Soc. Jpn.*, 75(1B), 181–189.
- Kurapov, A. L., J. S. Allen, G. D. Egbert, R. N. Miller, P. M. Kosro, M. Levine, and T. Boyd (2005a), Distant effect of assimilation of moored currents into a model of coastal wind-driven circulation off Oregon, *J. Geophys. Res.*, 110, C02022, doi:10.1029/2003JC002195.
- Kurapov, A. L., J. S. Allen, G. D. Egbert, R. N. Miller, P. M. Kosro, M. D. Levine, T. Boyd, and J. A. Barth (2005b), Assimilation of moored velocity data in a model of coastal wind-driven circulation off Oregon: Multivariate capabilities, *J. Geophys. Res.*, 110, C10S08, doi:10.1029/2004JC002493.
- Lewis, J. K., I. Shulman, and A. F. Blumberg (1998), Assimilation of doppler radar current data into numerical ocean models, *Cont. Shelf Res.*, 18(5), 541–559.
- Lynch, D. R., C. E. Naimie, and C. G. Hannah (1998), Hindcasting the Georges bank circulation. Part I: Detiding, *Cont. Shelf Res.*, 18(6), 607–639.
- Malanotte-Rizzoli, P. (Ed.) (1996), *Modern Approaches to Data Assimilation in Ocean Modeling*, Elsevier Science, 468 pp.
- McLaughlin, D. (2002), An integrated approach to hydrologic data assimilation: Interpolation, smoothing, and filtering, *Adv. Water Resour.*, 25(8–12), 1275–1286.
- Oke, P. R., J. S. Allen, R. N. Miller, G. D. Egbert, and P. M. Kosro (2002), Assimilation of surface velocity data into a primitive equation coastal ocean model, *J. Geophys. Res.*, 107(C9), 3122, doi:10.1029/2000JC000511.
- Raudsepp, U., D. Beletsky, and D. J. Schwab (2003), Basin scale topographic waves in the Gulf of Riga, *J. Phys. Oceanogr.*, 33, 1129–1140.
- Schwab, D. J. (1983), Numerical simulation of low-frequency current fluctuations in Lake Michigan, *J. Phys. Oceanogr.*, 13, 2213–2224.
- Schwab, D. J. (1992), A review of hydrodynamic modeling in the Great Lakes from 1950–1990 and prospects for the 1990's, in *Chemical Dynamics in Fresh Water Ecosystems*, edited by A. P. C. Gobas and A. McCorquodale, pp. 41–62, Lewis Publishers, Ann Arbor, MI.
- Stein, M. L. (1999), *Interpolation of Spatial Data: Some Theory for Kriging*, Springer.
- Stroud, J., B. Lesht, D. Schwab, D. Beletsky, and M. L. Stein (2006), Tracking suspended sediment motion in Lake Michigan by combining satellite images with a numerical model, *Tech. Rep. 38*, Center for Integrating Statistical and Environmental Science, Univ. of Chicago.
- Wahba, G., D. R. Johnson, F. Gao, and J. Gong (1995), Adaptive tuning of numerical weather prediction models: randomized gcv in three- and four-dimensional data assimilation, *Mon. Weather Rev.*, 123(11), 3358–3369.

D. Beletsky, CILER, SNRE, University of Michigan, Ann Arbor, MI, USA. (dima.beletsky@noaa.gov)

D. J. Schwab, Great Lakes Environmental Research Laboratory, NOAA, Ann Arbor, MI, USA. (david.schwab@noaa.gov)

M. L. Stein, Department of Statistics, University of Chicago, Chicago, IL, USA. (stein@galton.uchicago.edu)

Z. Zhang, CISES, 5734 S Ellis Avenue, Chicago, IL 60637, USA. (zpzhang@stanfordalumni.org)